# Diffuse-reflection boundary conditions for a thermal lattice Boltzmann model in two dimensions: Evidence of temperature jump and slip velocity in microchannels

Victor Sofonea[1,2,*] and Robert F. Sekerka[2,†]
[1]*Laboratory for Numerical Simulation and Parallel Computing in Fluid Mechanics, Center for Fundamental and Advanced Technical Research, Romanian Academy, Bd. Mihai Viteazul 24, RO-300223 Timişoara, Romania*
[2]*Department of Physics, Carnegie Mellon University, Pittsburgh, Pennsylvania 15213, USA*
(Received 14 December 2004; published 30 June 2005)

We discuss the implementation of diffuse reflection boundary conditions in a thermal lattice Boltzmann model for which the upwind finite difference scheme is used to solve the set of evolution equations recovered after discretization of the velocity space. Simulation of heat transport between two parallel walls at rest shows evidence of temperature jumps at the walls that increase with Knudsen number. When the walls move in opposite directions with speeds $\pm u_W$, fluid velocity slip is observed at the walls, together with temperature jumps.

DOI: 10.1103/PhysRevE.71.066709 PACS number(s): 47.11.+j, 47.45.−n, 51.10.+y

## I. INTRODUCTION

Implementations of *no-slip* boundary conditions are widely used in the lattice Boltzmann (LB) literature (see [1–4] and references therein). However, experimental and theoretical studies which date back to the time of Maxwell [5] and Smoluchowski [6] and were extended thereafter by many other scientists (see, for example, [7–9] and references therein), account for the existence of fluid temperature jumps and velocity slip near walls. Temperature jumps and velocity slip become noticeable when the Knudsen number Kn (defined as the ratio of the mean free path to the fluid system size) is large enough (typically $\mathrm{Kn} \geqslant 0.01$) and the continuum assumption in the derivation of the Navier-Stokes equations breaks down. This happens mainly at two extreme scales: high-speed high-altitude aerodynamics and micro/nanosize devices known as microelectromechanical systems (MEMS) [10,11]. Technological developments in these areas still require appropriate computer models to capture jump/slip phenomena at the walls, which may provide an alternative to molecular dynamics or direct simulation Monte Carlo models (the interested reader may refer to [8,11–14] and references therein for an overview of these models).

According to the *diffuse reflection* model [7,9,10,15], gas particles that strike a microscopically rough wall get reflected at some random angle that is uncorrelated with their angle of incidence. This is due to particle-wall interaction, which has the effect of assigning some information belonging to the wall to the reflected particles. The particles that leave the wall follow a Maxwellian distribution law, parametrized by the wall velocity $\mathbf{u}_W$ and the wall temperature $\theta_W$.

The purpose of this paper is to discuss the implementation of diffuse reflection boundary conditions for lattice Boltzmann models. For convenience, our discussion will refer to a recently introduced thermal finite difference lattice Boltzmann (FDLB) model with multiple speeds in two dimensions [16], which is briefly reviewed in Sec. II. Other FDLB models that are able to recover the correct conservation equations for mass, momentum and energy density from a single set of distribution functions, such as the discrete velocity model introduced in [17,18], may be considered as well. The relaxation time, as well as the definition of the mean free path and the Knudsen number are addressed in Sec. III. Implementation of the diffuse reflection boundary conditions for the thermal FDLB model is described in Sec. IV. To test our diffuse reflection boundary conditions, we considered the stationary solutions of two physical problems. The first one is the problem of heat transport between two parallel walls at rest. The second one is Couette flow between parallel oppositely moving walls having the same temperature. For these simple problems, approximate solutions based on continuum models for the temperature and velocity fields are derived in Sec. V and the existence of the temperature jump and velocity slip is discussed in connection with the ideas already developed by Maxwell and Smoluchowski. FDLB simulation results are reported in Sec. VI. The results show that both physical phenomena (temperature jump and velocity slip) are well recovered using the diffuse reflection boundary conditions.

## II. REVIEW OF THE THERMAL FDLB MODEL

The thermal FDLB model [16] is derived from the Boltzmann equation with the well-known Bhatnagar-Gross-Krook (BGK) collision term [1–4] using an appropriate procedure for the discretization of the velocity space. Three basic reference quantities may be used to express the Boltzmann equation in a nondimensionalized form. The first one is a characteristic length $l_R$ of the system, e.g., the width of the channel where the fluid is flowing. The second one is a reference mass $m_R$. For a single component fluid, the natural choice for $m_R$ is the mass of the fluid particles. The third quantity is a reference energy $e_R = k_B T_R$ where $k_B$ is Boltzmann's constant and $T_R$ is a reference temperature. The nondimensionalized temperature is $\theta = T/T_R$. All simulation results reported in this paper will be plotted in nondimensionalized form. The references for the following

*Electronic address: sofonea@acad-tim.tm.edu.ro
†Electronic address: rs07@andrew.cmu.edu

 

physical quantities are derived from the basic quantities mentioned above: speed $c_R=\sqrt{k_BT_R/m_R}$, time $t_R=l_R/c_R$, particle number density $n_R=1/l_R^3$, mass density $\rho_R=m_R/l_R^3$, specific heat $c_{pR}=k_B/m_R$, dynamical viscosity $\eta_R=m_Rc_R/l_R^2$ and thermal conductivity $\kappa_R=k_Bc_R/l_R^2$. Since the nondimensionalized mass of the fluid particles is assumed to be $m=1$, the nondimensionalized sound speed equals $c_S=\sqrt{\theta(D+2)/D}$, where $D=2$ is the dimension of the coordinate space.

The discretization procedure used in [16] involves a set of 33 nondimensionalized velocities $\{e_0, e_{ki}(k=1,\ldots 4, i=1,\ldots 8)\}$

$$e_0 = 0,$$

$$e_{ki} = \left[\cos\frac{\pi(i-1)}{4}, \sin\frac{\pi(i-1)}{4}\right] c_k, \tag{1}$$

where the values of $c_k$ are given by Eq. (8) below. The corresponding distribution functions $f_0=f_0(\mathbf{x},t)$, $f_{ki}=f_{ki}(\mathbf{x},t)$, $k=1,\ldots 4, i=1,\ldots 8$ evolve according to the following set of nondimensionalized equations:

$$\partial_t f_{ki} + \mathbf{e}_{ki}\cdot\boldsymbol{\nabla} f_{ki} = -\frac{1}{\tau}[f_{ki} - f_{ki}^{eq}]. \tag{2}$$

In this model, the equilibrium distribution functions $f_0^{eq}=f_0^{eq}(\mathbf{x},t)$, $f_{ki}^{eq}=f_{ki}^{eq}(\mathbf{x},t)$, $k=1,\ldots 4, i=1,\ldots,8$ are expressed using a series expansion $s_{ki}=s_{ki}(\theta,\mathbf{u})$ up to fourth order terms in the local fluid velocity $\mathbf{u}=\mathbf{u}(\mathbf{x},t)$, which has the Cartesian components $u_\alpha$, $\alpha=1,2$ (summation over repeated Greek indices is understood):

$$f_{ki}^{eq} = \rho F_k s_{ki}, \tag{3}$$

$$\begin{aligned} s_{ki} = {} & \left(1 - \frac{u^2}{2\theta} + \frac{u^4}{8\theta^2}\right) + \frac{1}{\theta}\left(1 - \frac{u^2}{2\theta}\right) e_{ki\xi}u_\xi \\ & + \frac{1}{2\theta^2}\left(1 - \frac{u^2}{2\theta}\right) e_{ki\xi}e_{ki\eta}u_\xi u_\eta + \frac{1}{6\theta^3} e_{ki\xi}e_{ki\eta}e_{ki\zeta}u_\xi u_\eta u_\zeta \\ & + \frac{1}{24\theta^4} e_{ki\xi}e_{ki\eta}e_{ki\zeta}e_{ki\chi}u_\xi u_\eta u_\zeta u_\chi. \end{aligned} \tag{4}$$

Here $\rho=\rho(\mathbf{x},t)$ is the local fluid density and $\theta=\theta(\mathbf{x},t)$ is the local temperature expressed in nondimensional form. The weight factors $F_k=F_k(\theta)$ that appear in Eq. (3) are expressed in [16] as functions of the local temperature $\theta$, as well as the speeds $c_k$, $k=1,\ldots,4$:

$$\begin{aligned} F_k = {} & \frac{1}{c_k^2(c_k^2 - c_{\{k+1\}}^2)(c_k^2 - c_{\{k+2\}}^2)(c_k^2 - c_{\{k+3\}}^2)} \\ & \times [48\theta^4 - 6(c_{\{k+1\}}^2 + c_{\{k+2\}}^2 + c_{\{k+3\}}^2)\theta^3 + (c_{\{k+1\}}^2 c_{\{k+2\}}^2 \\ & + c_{\{k+2\}}^2 c_{\{k+3\}}^2 + c_{\{k+3\}}^2 c_{\{k+1\}}^2)\theta^2 - c_{\{k+1\}}^2 c_{\{k+2\}}^2 c_{\{k+3\}}^2 \theta/4], \end{aligned} \tag{5}$$

$$F_0 = 1 - 8(F_1 + F_2 + F_3 + F_4). \tag{6}$$

Here we used the notation $(l=1,2,3)$

$$\{k+l\} = \begin{cases} k+l, & k+l \leqslant 4, \\ k+l-4, & k+l > 4. \end{cases} \tag{7}$$

The nondimensionalized values of the speeds $c_k$ $(k=1,\ldots 4)$ were determined in [16] by requiring the weight factors $F_k$ to be positive and calculating correct moments up to 6th order in $\mathbf{u}$ for the largest possible temperature range $(0.4 \leqslant \theta \leqslant 1.6)$:

$$\{c_k\} = \{1.0, 1.92, 2.99, 4.49\}. \tag{8}$$

The *collide and stream* philosophy of standard LB models [1–4], where particles move along the lattice links with the lattice velocity $c$, implies the close relationship $c=k\delta s/\delta t$ between the discretizations of both velocity and coordinate spaces ($k$ is an integer number, $\delta s$ is the lattice spacing and $\delta t$ is the time step). Such a relationship is no longer considered in finite difference lattice Boltzman (FDLB) models [19–23], which start directly from the Boltzmann equation and allow the freedom to use multispeed models, like the one defined by Eqs. (1) and (8). Standard LB models cannot handle discrete velocity sets like the one in Eq. (8), where the nondimensionalized velocities are no longer expressed as integer numbers. This justifies the use of finite difference numerical schemes for the evolution equations (2).

The thermal FDLB model allows one to recover the correct conservation equations for mass, momentum and energy density of an ideal gas [16], where dimensionless physical values of the transport coefficients $\eta$ (dynamic viscosity) and $\kappa$ (heat conductivity) are

$$\eta = \rho\theta\tau, \tag{9}$$

$$\kappa = 2\rho\theta\tau. \tag{10}$$

The value of the Prandtl number follows immediately (the nondimensionalized value of the specific heat at constant pressure is $c_p=2$ for the LB model used in this paper):

$$\mathrm{Pr} = \frac{c_p\eta}{\kappa} = 1. \tag{11}$$

## III. RELAXATION TIME, MEAN FREE PATH AND KNUDSEN NUMBER

The majority of single-component LB models in the literature use a constant value of the nondimensionalized relaxation time $\tau$ which appears in the evolution equations (2). The relaxation time $\tau$ is related to the nondimensionalized mean free path through

$$\lambda = \tau\bar{c} \tag{12}$$

where $\bar{c}$ is the nondimensionalized average speed of the fluid particles. According to kinetic theory [7], the average speed $\bar{c}$ is always proportional to $\sqrt{\theta}$. In the two-dimensional case, we have

$$\bar{c} = \sqrt{\pi\theta/2}. \tag{13}$$

However, for the thermal LB model we use in this paper, we prefer to use the direct definition of the local average speed:

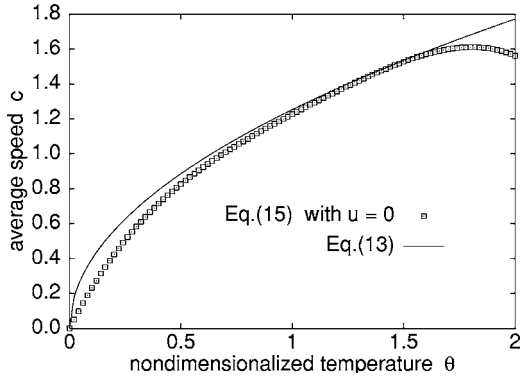


FIG. 1. Temperature dependence of the nondimensionalized average speed, Eq. (15) for $\mathbf{u}=0$. The continuous line shows the theoretical result of the kinetic theory, Eq. (13), and is provided for comparison.

$$\bar{c} = \frac{\sum_{k=1}^{4} c_k \sum_{i=1}^{8} f_{ki}}{f_0 + \sum_{k=1}^{4} \sum_{i=1}^{8} f_{ki}}. \tag{14}$$

An alternative definition of $\bar{c}$ involving the equilibrium distribution functions $f_{ki}^{eq}$ instead of $f_{ki}$ in the equation above was found to give similar results during our computer simulations. The use of $f_{ki}^{eq}$ instead of $f_{ki}$ in Eq. (14) gives the following expression of the average speed $\bar{c}$, which is found to dependent on the local temperature $\theta$, as well as the local fluid velocity $\mathbf{u}$

$$\bar{c} = \sum_{k=1}^{4} c_k F_k \left[ 8 - 2u^2 \left( \frac{2}{\theta} - \frac{c_k^2}{\theta^2} \right) + u^4 \left( \frac{1}{\theta^2} - \frac{c_k^2}{\theta^3} + \frac{c_k^4}{8\theta^4} \right) \right]. \tag{15}$$

The unphysical dependence of the average speed $\bar{c}$ on the local fluid velocity $\mathbf{u}$ is a consequence of the series expansion (4) of the Maxwellian equilibrium distribution function, which results in the loss of Galilean invariance. However, the effect of the local fluid velocity on the average speed is negligible for small values of Mach's number $\mathrm{Ma}=u/c_S$. If we use Eq. (15) to plot the temperature dependence of the average speed $\bar{c}$ for $\mathbf{u}=0$ (Fig. 1), we see that in the temperature range $0.4 \leqslant \theta \leqslant 1.6$ where the model [16] is supposed to be valid, the resulting curve is close enough to the theoretical expression (13), which was derived using kinetic theory. This strongly supports the capability of the thermal LB model introduced by Watari and Tsutahara [16] to properly capture physical phenomena where the mean free path and the corresponding nonvanishing value of the Kundsen number play an important role.

As mentioned previously, the reference length $l_R$ usually equals the size $\tilde{L}$ of the fluid system (e.g., the channel width). Consequently, when $\tau$ is a constant simulation parameter, the local Knudsen number is (dimensionalized quantities carry the tilde symbol)

$$\mathrm{Kn}_\tau = \frac{\tilde{\lambda}}{\tilde{L}} = \lambda = \tau \bar{c}. \tag{16}$$

Then according to Eq. (13), we will have $\mathrm{Kn}_\tau \propto \sqrt{\theta}$.

When $\tau$ is not a constant simulation parameter, we proceed as follows: According to kinetic theory, the mean free path is inversely proportional to the dimensionless particle density. We therefore allow $\tau$ to be a variable and define a Knudsen number

$$\mathrm{Kn}_\Lambda = \frac{\tilde{\lambda}}{\tilde{L}} = \lambda = \frac{\Lambda}{n}, \tag{17}$$

where $\Lambda$ is a dimensionless constant. The constant $\Lambda$ depends on the nondimensionalized particle diameter $d$ [7,24]:

$$\Lambda = \frac{1}{\sqrt{2}\pi d^2}. \tag{18}$$

Since the physical value $\tilde{d}$ of the particle diameter is always smaller than the reference length $l_R$ (which is usually the channel width), the nondimensionalized value of the constant $\Lambda$ is expected to exceed the unit value by several orders of magnitude. When considering a typical capillary channel, we may take $l_R = 10^{-6}$ m or $l_R = 10^{-3}$ m. For $\tilde{d}$ of the order of a few nanometers, we get $\Lambda \simeq 1.0 \times 10^6$ and $\Lambda \simeq 1.0 \times 10^{12}$, respectively.

In order to preserve the relation (12) for a hard sphere gas, the nondimensionalized relaxation time $\tau$ should be dependent on the local particle density $n$, as well as the average speed $\bar{c}$ defined by Eq. (14):

$$\tau = \frac{\Lambda}{n\bar{c}}. \tag{19}$$

According to kinetic theory where $\bar{c} \propto \sqrt{\theta}$, the relaxation time (19) is more realistic than the constant relaxation time since it gives a dynamic viscosity which is density independent and follows a nonlinear dependence on temperature, $\eta \propto \sqrt{\theta}$ [7]. For isothermal fluid systems, the relaxation time (19) reduces to the density-dependent relaxation time $\tau \propto 1/n$ of the split collision term introduced in [25]. Since the distribution functions $f_{ki}$ defined in each lattice node change with temperature, the average speed (14) is still temperature dependent.

In the present paper, we will report simulation results recovered using both versions of the relaxation time, the constant one and the density-dependent relaxation time (19). We will refer to the corresponding Knudsen number, Eqs. (16) and (17), respectively, when discussing the simulation results for each case.

## IV. DIFFUSE REFLECTION BOUNDARY CONDITIONS

The thermal FDLB model [16], as originally developed by its authors, uses the second order upwind finite difference scheme to solve the evolution equations (2) in the two-dimensional space. A square lattice $\mathcal{L}$ was used to perform the space discretization. Thermal Couette flow was successfully simulated using this model and no-slip boundary conditions [16]. For this purpose, lattice boundary nodes were located on the channel walls and an extrapolation method [26,27] was used to provide the values of the distribution

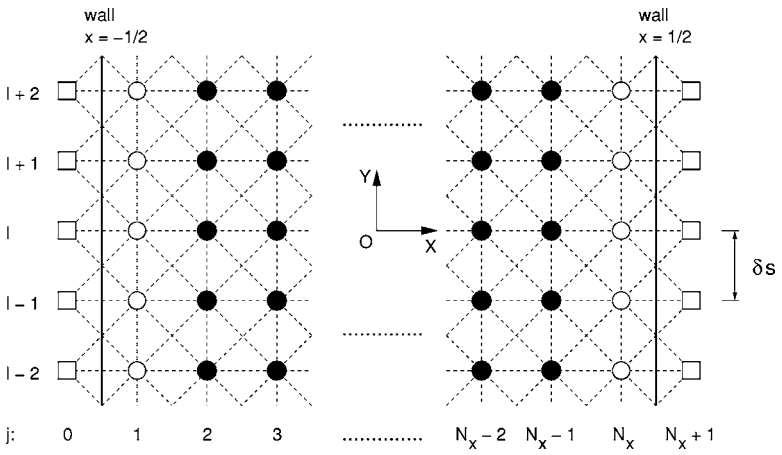


FIG. 2. The square lattice used for finite difference LB simulation of channel flow: ●, bulk nodes; ○, boundary nodes; □, ghost nodes outside the walls. Walls are situated at half lattice spacing between boundary nodes and ghost nodes. Periodic boundary conditions are used in the vertical direction.

functions in these nodes. This procedure forces the fluid's temperature and velocity (defined in the lattice boundary nodes) to equal the wall's temperature and velocity, respectively.

In this paper, we adopt a different strategy already used by other authors and place the channel walls at half lattice spacing *outside* the boundary nodes [28–30], as shown in Fig. 2. We preserve the forward Euler difference to compute the time derivative in (2), as done in [16], but we switch to the first order upwind scheme on the characteristic line in order to compute the effect of the operator $\mathbf{e}_{ki}\cdot\nabla$ on the distribution function $f_{ki}$ [23]. Besides better numerical stability in the presence of density gradients [31,32], the first order upwind scheme, which involves information from two lattice nodes on each characteristic line, may be easily handled on the boundaries since this scheme requires only a single row of ghost nodes to be introduced outside the walls, as described below. According to the upwind scheme, the distribution functions defined at time $t$ in the node $\mathbf{x}$ of the square lattice $\mathcal{L}$ are updated as follows:

$$f_{ki}(\mathbf{x},t+\delta t) = f_{ki}(\mathbf{x},t) - \frac{1}{\tau}[f_{ki}(\mathbf{x},t) - f_{ki}^{eq}(\mathbf{x},t)] - \frac{c_k\delta t}{\delta s}[f_{ki}(\mathbf{x},t) - f_{ki}(\mathbf{x}-A_i\delta s\mathbf{e}_{ki}/c_k,t)]. \quad (20)$$

Here $\delta s$ is the lattice spacing, $\delta t$ is the time step and the constants $A_i$ are given by

$$A_i = \begin{cases} 1, & i = 1,3,5,7, \\ \sqrt{2}, & i = 2,4,6,8. \end{cases} \quad (21)$$

Application of the updating rule (20) in the *bulk nodes* of the square lattice in Fig. 2 is straightforward. The same holds for lattice nodes where periodic boundary conditions in the $y$ direction apply. Special attention should be paid when updating the distribution functions in the *boundary nodes* of the lattice (i.e., those fluid nodes located near the channel wall, which have the $x$ index $j=1$ or $j=N_x$ in Fig. 2) since the distribution functions $f_{ki}(\mathbf{x}-A_i\delta s\mathbf{e}_{ki}/c_k,t)$ are not defined for certain values of the index $i$. The *ghost nodes* where these distribution functions should be evaluated (i.e., the lattice nodes with $j=0$ or $j=N_x+1$) are outside the walls at half lattice spacing and we must provide appropriate handling rules.

For convenience, we refer to the ghost node $(0,l)$ located near the left channel wall. According to the *diffuse reflection* concept, the distribution functions defined in the boundary nodes $(1,l-1)$, $(1,l)$ and $(1,l+1)$ shown in Fig. 3, whose corresponding velocity vectors point towards the ghost node $(0,l)$, mix together (i.e., "thermalize"). The mixing process gives rise to new values of the distribution functions $f_{ki}^{0,l}$ ($k=1,\ldots,4, i=1,2,8$) defined in the ghost node $(0,l)$. These new values carry the information related to the wall temperature $\theta_W$ and the wall velocity $\mathbf{u}_W$. When the fluid density at the wall $\rho_W$ has no variation along the $y$ direction (as is the case for Couette flow), the requirement that the distribution functions follow the Maxwellian distribution law on the walls reads

$$\frac{f_{k1}^{0,l}+f_{k1}^{1,l}}{F_k(\theta_W)s_{k1}(\theta_W,\mathbf{u}_W)} = \frac{f_{k2}^{0,l}+f_{k2}^{1,l+1}}{F_k(\theta_W)s_{k2}(\theta_W,\mathbf{u}_W)} = \frac{f_{k8}^{0,l}+f_{k8}^{1,l-1}}{F_k(\theta_W)s_{k8}(\theta_W,\mathbf{u}_W)} = 2\rho_W, \quad k=1,\ldots,4. \quad (22)$$

Equations. (22), together with the requirement that there is no mass flux perpendicular to the wall

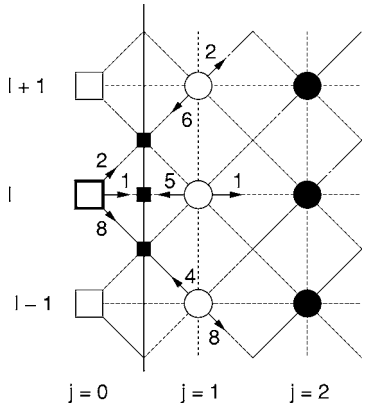


FIG. 3. Diffuse reflection procedure: □, ghost nodes; ○, boundary nodes; ■, wall points where the distribution functions $f_{ki}$ ($i=1,2,8$) follow the Maxwellian distribution law.

$$\sum_k c_k \left[ f_{k5}^{1,l} + \frac{\sqrt{2}}{2}(f_{k4}^{1,l-1} + f_{k6}^{1,l+1}) \right] = \sum_k c_k \left[ f_{k1}^{0,l} + \frac{\sqrt{2}}{2}(f_{k2}^{0,l} + f_{k8}^{0,l}) \right] \tag{23}$$

may be solved to get the values of the distribution functions in the ghost node $(0,l)$ after each time step.

## V. COUETTE FLOW IN MICROCHANNELS: TEMPERATURE JUMP AND VELOCITY SLIP

In order to have some basis for comparison of our simulations, we need approximate analytical solutions for two fluid flow problems that we later simulate using the thermal FDLB model with the diffuse reflection boundary conditions. For this purpose, we solve the classical continuum equations (Navier-Stokes-Fourier) for the average fluid velocity and temperature fields. We consider a fluid confined between two infinite walls located at $x=\pm 1/2$, which are parallel to the $y$ axis. The left and right walls move along the $y$ axis with constant speeds $u_{WL}$ and $u_{WR}$, respectively. Their temperatures are $\theta_{WL}$ and $\theta_{WR}$. We restrict ourselves to the stationary case and assume that the $x$ component of the fluid velocity vanishes. In this case, the nondimensionalized density $(\rho)$, temperature $(\theta)$ and velocity $(u_y \equiv u)$ fields depend only on the $x$ coordinate and the conservation equations recovered from the FDLB evolution equations (2) using the method of moments [16] become

$$\partial_x(\rho\theta) = 0, \tag{24}$$

$$\partial_x[\eta(\partial_x u)] = 0, \tag{25}$$

$$\partial_x[\kappa(\partial_x \theta)] + \partial_x[\eta u(\partial_x u)] = 0. \tag{26}$$

When using a constant relaxation time $\tau$, the transport coefficients $\eta$ and $\kappa$ are found to be constant since the fluid pressure $\rho\theta$ is constant according to Eq. (24). If local temperature has no large variations in the fluid system (as will frequently happen in the FDLB simulations reported in this paper), the assumption of constant values of the transport coefficients may be considered as an approximation in the case of the relaxation time provided by Eq. (19).

To get the temperature and the velocity profile across the channel by solving Eqs. (25) and (26), we need to provide the necessary boundary conditions. We follow the ideas of Maxwell and Smoluchowski [5,6], as well as the outlines in [8,24,33] and write the exprressions of the temperature jumps and velocity slips at the left $(L)$ and right walls $(R)$ respectively, to the first order in the Knudsen number:

$$\theta_L^{jump} = \theta_{FL} - \theta_{WL} = \frac{2\gamma}{\gamma+1}\frac{1}{\mathrm{Pr}}\left[\mathrm{Kn}\frac{\partial\theta}{\partial x}\right]_{FL}, \tag{27a}$$

$$\theta_R^{jump} = \theta_{WR} - \theta_{FR} = \frac{2\gamma}{\gamma+1}\frac{1}{\mathrm{Pr}}\left[\mathrm{Kn}\frac{\partial\theta}{\partial x}\right]_{FR}, \tag{27b}$$

$$u_L^{slip} = u_{FL} - u_{WL} = \left[\mathrm{Kn}\frac{\partial u}{\partial x}\right]_{FL}, \tag{28a}$$

$$u_R^{slip} = u_{WR} - u_{FR} = \left[\mathrm{Kn}\frac{\partial u}{\partial x}\right]_{FR} \tag{28b}$$

($\gamma = c_p/c_v$ is the adiabatic coefficient; for the LB model considered in this paper, $\gamma=2$). The indices $FL$ and $FR$ in the relations above refer to the values of the corresponding quantities evaluated in the fluid at the left $(x=-1/2)$ and right walls $(x=1/2)$, respectively.

We now assume that the density and temperature variations across the channel are small enough for the value of the Knudsen number to be considered constant. If we assume that the velocity profile across the channel is linear and search for the solutions $u=u(x)$ and $\theta=\theta(x)$ of Eqs. (25) and (26) in the form

$$u(x) = Ax + B, \tag{29a}$$

$$\theta(x) = Cx^2 + Dx + E, \tag{29b}$$

we get

$$A = \frac{u_{WR} - u_{WL}}{1 + 2\mathrm{Kn}}, \tag{30a}$$

$$B = \frac{u_{WR} + u_{WL}}{2}, \tag{30b}$$

$$C = -\frac{\eta}{2\kappa}A^2, \tag{30c}$$

$$D = \frac{\theta_{WR} - \theta_{WL}}{1 + 2h\mathrm{Kn}}, \tag{30d}$$

$$E = \frac{\theta_{WR} + \theta_{WL}}{2} + \frac{\eta}{8\kappa}A^2(1 + 4h\mathrm{Kn}), \tag{30e}$$

where

$$h = \frac{2\gamma}{\gamma+1}\frac{1}{\mathrm{Pr}}. \tag{31}$$

For the LB model considered in this paper, we have $h=1.33$.

To test our diffuse reflection boundary conditions and to compare the FDLB simulation results with the analytical results, Eqs. (29a) and (30e), we further restrict ourselves to two particular cases. The first one is the stationary heat transport problem between two parallel walls at rest. In this case, we have $u_{WR}=u_{WL}=0$ and Eq. (29b) reduces to

$$\theta(x) = \frac{\theta_{WR} - \theta_{WL}}{1 + 2h\mathrm{Kn}}x + \frac{\theta_{WR} + \theta_{WL}}{2}. \tag{32}$$

The temperature jumps at the left and right walls are immediately recovered from Eqs. (27a), (27b), and (32):

$$\theta_L^{jump} = \frac{\theta_{WR} - \theta_{WL}}{2}\frac{2h[\mathrm{Kn}]_{FL}}{1 + 2h[\mathrm{Kn}]_{FL}}, \tag{33a}$$

$$\theta_R^{jump} = \frac{\theta_{WR} - \theta_{WL}}{2} \frac{2h[\mathrm{Kn}]_{FR}}{1 + 2h[\mathrm{Kn}]_{FR}}. \tag{33b}$$

The temperature jumps at the walls become negligible only for small values of the Knudsen number.

Note that Kn is constant in Eqs. (30a), (30d), and (30e). In Eqs. (33a) and (33b) we have restored subscripts *FL* and *FR* as an approximation since local values of Kn are likely to lead to better accuracy.

The second physical problem we consider here is thermal Couette flow in the stationary state. For convenience, we set $u_{WR} = -u_{WL} = u_W$ and $\theta_{WR} = \theta_{WL} = \theta_W$. The velocity and temperature profiles across the channel are still given by Eqs. (29a) and (29b) with $B=0$ and $D=0$. The velocity slip and the temperature jump at the walls are

$$u_L^{slip} = u_W \frac{2[\mathrm{Kn}]_{FL}}{1 + 2[\mathrm{Kn}]_{FL}}, \tag{34a}$$

$$u_R^{slip} = u_W \frac{2[\mathrm{Kn}]_{FR}}{1 + 2[\mathrm{Kn}]_{FR}}, \tag{34b}$$

$$\theta_L^{jump} = u_W^2 \frac{h[\mathrm{Kn}]_{FL}}{(1 + 2[\mathrm{Kn}]_{FL})^2}, \tag{35a}$$

$$\theta_R^{jump} = -u_W^2 \frac{h[\mathrm{Kn}]_{FR}}{(1 + 2[\mathrm{Kn}]_{FR})^2}. \tag{35b}$$

The equations above express the fact that Couette flow exhibits no observable velocity slip and temperature jump at the walls when the Knudsen number is small enough. Note that in Couette flow the fluid has a higher temperature at the walls than the walls themselves. This arises because heat is generated by viscous flow within the fluid. In the previous case (33a) and (33b) when the walls were at rest, there was only heat conduction and no viscous dissipation within the fluid.

The Navier-Stokes-Fourier equations are for a continuum model, so they are always an approximation to a system of particles. We only use them as a basis of Eqs. (32)–(35) to compare our simulation results with, and not in the simulation themselves. It is only a question of accuracy to state a Knudsen number below which the Navier-Stokes-Fourier equations are valid. According to literature, it is generally believed that a Knudsen number less than 0.1 will suffice [8–11].

## VI. FDLB SIMULATION RESULTS

### A. Simulation parameters

Two series of FDLB simulations were done to investigate the effect of the diffuse reflection boundary conditions introduced in Sect. IV. As mentioned in the previous section, the first series refers to stationary heat transport between two parallel walls at rest, while the second one refers to stationary Couette flow between walls having the same temperature. In both cases, we used a two-dimensional lattice with $N_x = 100$ and $N_y = 5$ nodes with periodic boundary conditions along the *y* direction. Because of periodic boundary conditions in the *y* direction, any integer number $N_y \geqslant 1$ should work as well, but we preferred to design and test a true two-dimensional code to be used for future applications, e.g., long channels with customized $N_y$. Columns of ghost nodes were added outside the left and right wall, respectively (Fig. 2).

In the initial state, the lattice was filled with a homogeneous fluid of nondimensionalized particle density $n_{initial}$ and nondimensionalized temperature $\theta_{initial}$. Simulations were started using the same values of $n_{initial}$ and $\theta_{initial}$ for both versions of the relaxation time. For simulations done with the density-dependent relaxation time (19), we used the values $\Lambda = 1.0 \times 10^6$ and $\Lambda = 1.0 \times 10^{12}$. Since the results were qualitatively similar, in this paper we will refer only to the results recovered for $\Lambda = 1.0 \times 10^6$, which corresponds to a MEMS system size $l_R \simeq 10^{-6}$ m. Because the density of a gas under normal conditions is approximately $3 \times 10^{25}$ particles/m$^3$, we used the following set of nondimensionalized values of the fluid density in the initial state in order to achieve various values of the Knudsen number during our computer runs:

$$\{n_{initial}\} = \{10^9, 10^8, 5.0 \times 10^7, 3.3 \times 10^7, 2.5 \times 10^7, 2 \times 10^7\}. \tag{36}$$

The above values correspond to the following values of the Knudsen number in the initial state:

$$\{\mathrm{Kn}_{initial}\} = \{0.001, 0.01, 0.02, 0.03, 0.04, 0.05\}. \tag{37}$$

To achieve similar values of the Knudsen numbers in the initial state when using the constant relaxation time, the corresponding values of the constant relaxation time $\tau$ were always computed using Eqs. (13) and (16). E.g., for $\theta_{initial} = 1.0$ and the values of $n_{initial}$ given by Eq. (36), the corresponding values of $\tau$ are

$$\{\tau\} = \{0.0008, 0.008, 0.016, 0.024, 0.032, 0.040\}. \tag{38}$$

According to this strategy, the results recovered using the two versions of the relaxation time are expected to differ only when the fluid density changes significantly across the channel width.

The initial fluid temperature was always $\theta_{initial} = 1.0$ when investigating the heat transport problem (in this case, the left and right wall have different temperatures). The initial value of the fluid temperature was set equal to the wall temperature $\theta_W = 1.0$ when simulating Couette flow. We always performed 500,000 iterations with time step $\delta t = 10^{-4}$ to achieve the stationary state before plotting the results.

### B. Stationary heat transport problem

Figure 4 shows the stationary profiles of various quantities, which were computed for $n_{initial} = 2 \times 10^7$, $\theta_{WL} = 0.50$, $\theta_{WR} = 1.50$. In this case, the density variation across the channel is very large [Fig. 4(a)] and the differences between simulation results recovered using the two versions of the relaxation time are noticeable for the following quantities:

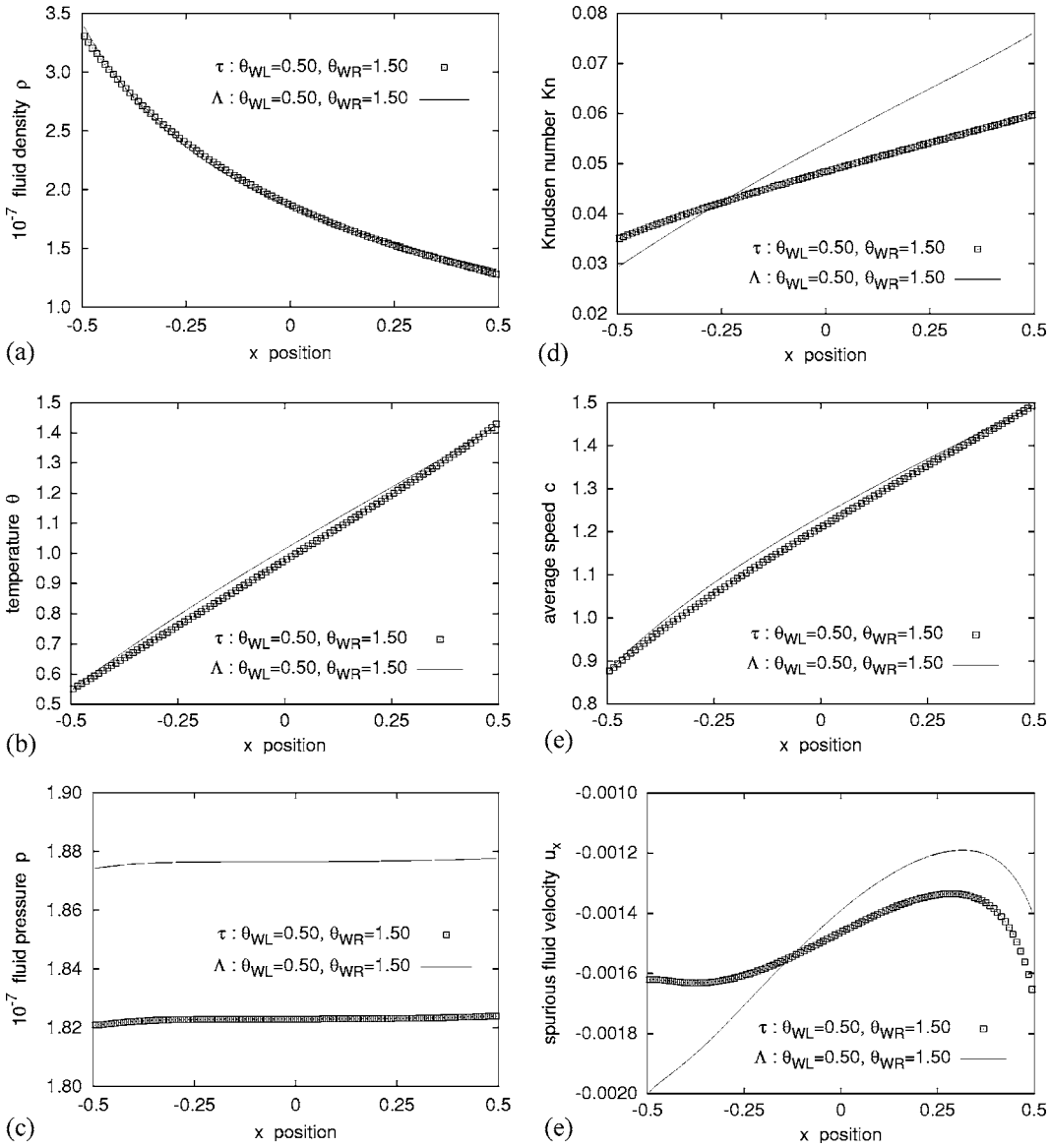


FIG. 4. Heat transport between two parallel walls at rest—stationary profiles of various nondimensionalized quantities, for $n_{initial}=2\times10^7$, $\theta_{WL}=0.50$, $\theta_{WR}=1.50$: (a) density, (b) temperature, (c) pressure, (d), Knudsen number, (e) average speed $\bar{c}$, and (f) spurious velocity $u_x$. Results recovered using the constant relaxation time carry the symbol $\tau$ while results recovered using the density dependent relaxation time defined by Eq. (19) carry the symbol $\Lambda$.

temperature [Fig. 4(b)], pressure [Fig. 4(c)], Knudsen number [Fig. 4(d)] and average speed [Fig. 4(e)]. When the difference between the right and left wall temperatures ($\theta_{WL}$ and $\theta_{WR}$) becomes small enough with respect to their mean value $\theta=1.0$, the differences between the results recovered using the two versions of the relaxation time become negligible.

According to Eq. (24), the fluid pressure is expected to be constant. Figure 4(c) shows the pressure profiles established between the walls for both versions of the relaxation time. The variation of the pressure near the walls is found to be less than 0.5% the mean value. However, the pressures recovered using the two versions of the relaxation time differ by nearly 3% when $\theta_{WL}=0.50$ and $\theta_{WR}=1.50$. In this case, the two versions of the relaxation time give noticeable differences also for the profiles of the temperature and average speed [Figs. 4(b) and 4(e)]. This is different from the case $\theta_{WL}=0.90$, $\theta_{WR}=1.10$, when the pressure profiles recovered using both versions of the relaxation time differ only by 0.1%.

A characteristic of the first order upwind scheme used in this paper, which plagues the simulation results is the presence of a spurious velocity $u_x$ in the regions where the $x$ component of the density gradient is not negligible [34]. The profiles of the spurious velocity $u_x$ are shown in Fig. 4(f). Even for the case $\theta_{WL}=0.50$, $\theta_{WR}=1.50$, the spurious velocity is found to be negligible with respect to the sound velocity $c_S=\sqrt{2\theta}$. Reduction of the spurious velocity may be achieved using higher order finite difference schemes or flux limiter schemes [35,36]. However, higher order schemes involve more than two lattice nodes on the characteristic line and the implementation of the diffuse reflection boundary conditions becomes more elaborate.

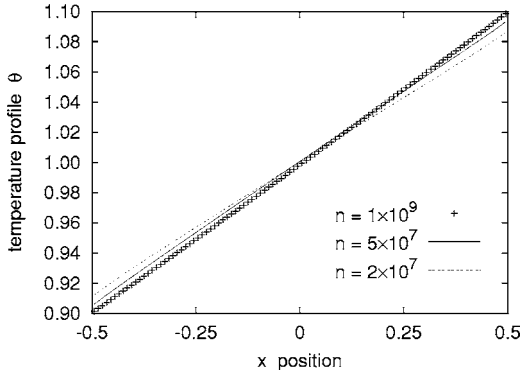


FIG. 5. Heat transport between two parallel walls at rest: nondimensionalized temperature profiles recovered in the stationary state using the density dependent relaxation time $\tau$ given by Eq. (19), for $\theta_{WL}=0.90$, $\theta_{WR}=1.10$ and three values of the initial fluid density $n$.

Figure 5 shows the stationary temperature profiles established between the rest walls for $\theta_{WL}=0.90$, $\theta_{WR}=1.10$ and various values of the initial (mean) density of the fluid, when the density dependent relaxation time is used. The temperature jumps near the walls are clearly seen when the mean fluid density decreases and the Knudsen number becomes large enough. Note that the temperature jumps near the left and right wall seem to be approximatively equal when the difference between the corresponding wall temperatures is small and the assumptions in Sec. V apply. In this case, the temperature profiles are quite linear and we expect Eqs. (32), (33a), and (33b) to be valid. To check this, we computed the local fluid temperatures and Knudsen numbers near the left and right walls respectively using linear extrapolation of the corresponding values in the adjacent lattice nodes. The results are plotted in Fig. 6 and compared to the analytical formulae, Eqs. (33a) and (33b). The agreement between the simulation results and the theory is excellent for $\theta_{WL}=0.90$, $\theta_{WR}=1.10$ [Fig. 6(a)], for both versions of the relaxation time.

For wall temperatures $\theta_{WL}=0.50$, $\theta_{WR}=1.50$, the values of the temperature jumps in Fig. 6(b) show some deviation from the analytical formulae, Eqs. (33a) and (33b). For these values of the wall temperatures, the fluid temperature profiles in Fig. 4(b), which were recovered using the density dependent relaxation time given by Eq. (19), are no longer linear. However, the fluid temperature profiles recovered using the constant relaxation time are still approximately linear in this case, as seen in Fig. 4(b), because of constant values of the transport coefficients. The assumption of constant values of the transport coefficients explains why the results in Fig. 6(a) are well superposed for both versions of the relaxation time. As previously mentioned in Sec. V, we do not expect the analytical results, Eqs. (32), (33a), and (33b), to be still valid when the difference between the wall temperatures is considerable with respect to their mean value. In this case, the values of the temperature jumps recovered using the constant relaxation time and those recovered using the density dependent relaxation time differ significantly [Fig. 6(b)].

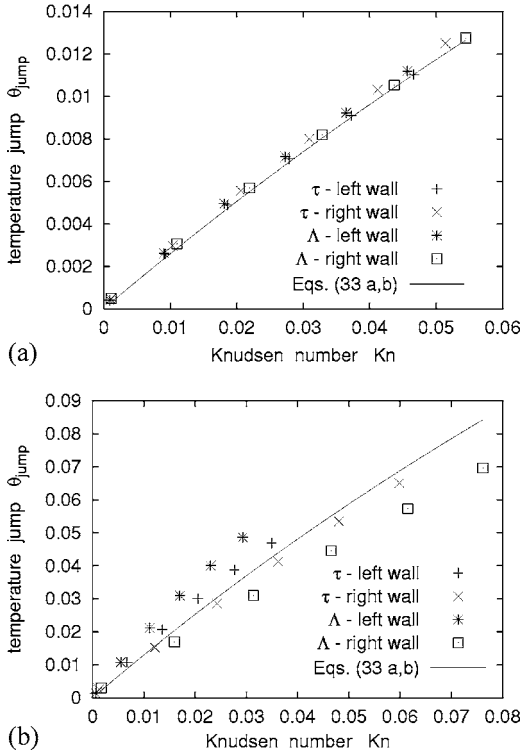


FIG. 6. Heat transport between two parallel walls at rest: Knudsen number dependence of temperature jumps at the left and right walls, recovered using both versions of the relaxation time. Results recovered using the constant relaxation time carry the symbol $\tau$ while results recovered using the variable relaxation time defined by Eq. (19) carry the symbol $\Lambda$. Wall temperatures are (a) $\theta_{WL}=0.90$, $\theta_{WR}=1.10$; (b) $\theta_{WL}=0.50$, $\theta_{WR}=1.50$.

### C. Couette flow

Figures 7(a) and 7(b) show the linear velocity profiles and the parabolic temperature profiles established between two parallel walls moving in the opposite directions ($u_W=0.1$ and $\theta_W=1.0$), for both versions of the relaxation time. The slip velocity and the temperature jump near the walls are clearly seen when the Knudsen number is large enough. Since there are no large variations of the temperature and fluid density across the channel in Couette flow, the results recovered using the two versions of the relaxation time are similar in this case.

It is worthwile to compare our parabolic temperature profiles in Fig. 7(b) and the corresponding profiles recovered by Watari and Tsutahara [16], which place the lattice boundary nodes on the channel walls. These authors use a different method to impose boundary conditions [26,27] and plot the profile of the nondimensionalized energy per particle, which is equivalent to temperature. For various values of the relaxation time, the temperature profiles recovered by Watari and Tsutahara for Couette flow are indistinguishable and temperature jumps are never observed near the walls.

Figure 8 show the dependence of the temperature jump and velocity slip on the value of the Knudsen number, for wall velocity $u_W=0.5$ and three values of the wall temperature. Results in this figure were recovered using both versions of the relaxation time. The values of the temperature

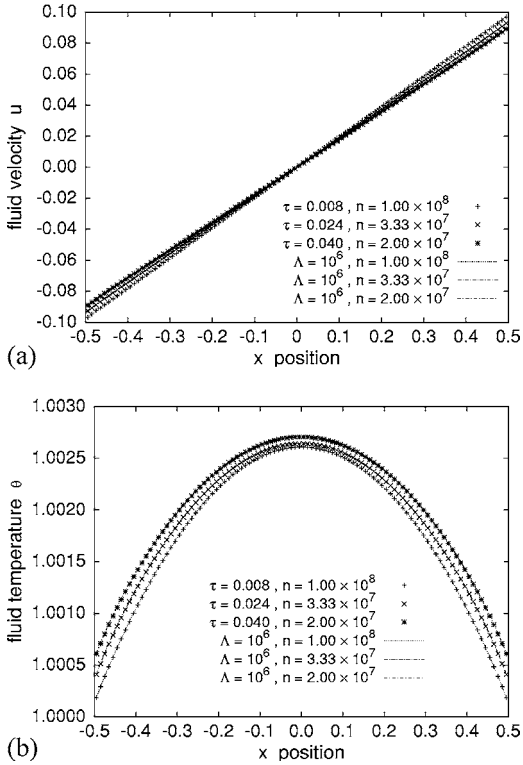


FIG. 7. Couette flow: (a) velocity profiles and (b) temperature profiles recovered using both versions of the relaxation time for wall temperatures $\theta_{WR}=\theta_{WL}=1.00$ and velocities $u_{WR}=-u_{WL}=0.1$. Results recovered using the constant relaxation time carry the symbol $\tau$ while results recovered using the variable relaxation time defined by Eq. (19) carry the symbol $\Lambda$.

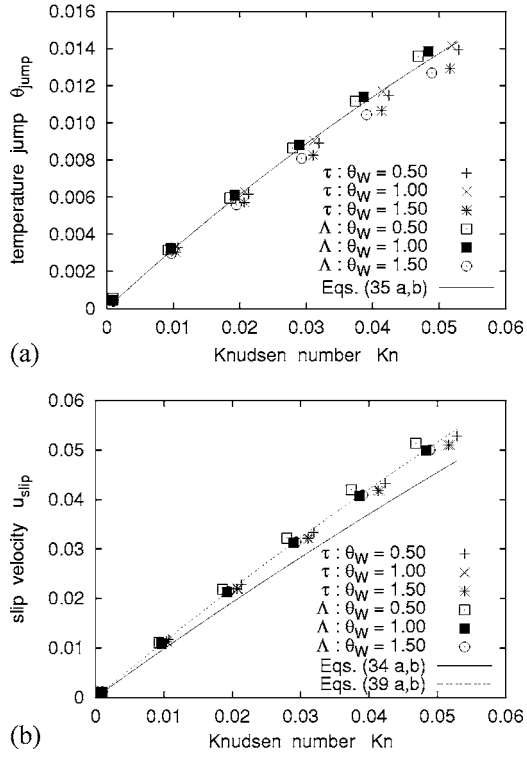


FIG. 8. Couette flow: effect of Knudsen number on the temperature jump (a) and velocity slip (b) for $u_W=0.5$ and three values of the wall temperature. Results recovered using the constant relaxation time carry the symbol $\tau$ while results recovered using the variable relaxation time defined by Eq. (19) carry the symbol $\Lambda$.

jumps are found to be in good agreement with the analytical results, Eqs. (35a) and (35b) derived in Sec. V. Concerning the dependence of the velocity slip on the Knudsen number, our simulation results suggest that there should be an extra factor $\zeta$ which multiplies the Knudsen number in Eqs. (34a) and (34b):

$$u_L^{slip} = u_W \frac{2\zeta[\mathrm{Kn}]_{FL}}{1+2\zeta[\mathrm{Kn}]_{FL}}, \tag{39a}$$

$$u_R^{slip} = u_W \frac{2\zeta[\mathrm{Kn}]_{FR}}{1+2\zeta[\mathrm{Kn}]_{FR}}. \tag{39b}$$

If the value $\zeta \approx 1.15$ is used, we obtain a better fit to the simulations of velocity slip, as shown in Fig. 8(b). This $\zeta$ factor might be related to different definitions of the mean free path and the fact that the mean free path for energy transport might differ from that of momentum transport. However, in view of the approximations involved in Eqs. (27) and (28) and the analytical solutions, this agreement may be fortuitous.

## VII. CONCLUSIONS

Diffuse reflection boundary conditions for the thermal finite difference lattice Boltzmann model with multiple speeds [16] were introduced in this paper. These conditions account for the redistribution of fluid particles which hit the walls such that the reflected particles carry some information from the wall. Their distribution functions depend on the wall's temperature and velocity. A square lattice is used to solve the set of evolution equations recovered after discretization of the velocity space and we used the first order upwind scheme to calculate the space derivatives. The distribution functions of the reflected particles are defined in ghost nodes outside the flow domain such that the channel walls are placed at half lattice spacing between the ghost nodes and the boundary nodes of the lattice.

In this paper, we also introduced a nondimensionalized relaxation time that is dependent on the local particle number density, as well as the local average speed of the fluid particles, Eq. (14). This relaxation time provides an alternative to the constant relaxation time used in the lattice Boltzmann literature. The two relaxation times give qualitatively similar results when the nondimensionalized density and temperature do not differ much from their average values in the fluid system.

FDLB simulations done using the diffuse reflection boundary conditions and both versions of the relaxation time (constant or density dependent) were carried out for two test problems: stationary heat transport between two parallel walls at rest and Couette flow between walls having the same temperature. In both test problems, temperature jumps at the walls become noticeable when the Knudsen number exceeds the value 0.001. Slip velocity accompanies the temperature

jump in Couette flow. The effect of the local Knudsen number on the temperature jump and slip velocity observed during the FDLB simulations was found to agree approximately with the theories of Maxwell and Smoluchowski.

Finally, we note that our boundary conditions were established under the assumption that there is no tangential component of the fluid density gradient near the wall. Further work is necessary to incorporate the general case when fluid density, as well as temperature, are allowed to vary along the wall. This would allow us to use FDLB models in order to investigate rarefaction effects in pressure-driven microscale flow, as well as less common phenomena such as thermal transpiration [8].

## ACKNOWLEDGMENTS

This work was supported by the NASA OBPR grant NNM04AA16G. V.S. acknowledges also the support of the Romanian Academy (grant GAR 416/2003-2004). Computer runs were done using the Portable Extensible Toolkit for Scientific Computation (PETSc 2.2.1) developed at Argonne National Laboratory, Argonne, Illinois [37].

[1] D. H. Rothman and S. Zaleski, *Lattice Gas Cellular Automata: Simple Models of Complex Hydrodynamics* (Cambridge University Press, Cambridge, England, 1997).
[2] B. Chopard and M. Droz, *Cellular Automata Modeling of Physical Systems* (Cambridge University Press, Cambridge, England, 1998).
[3] D. A. Wolf-Gladrow, *Lattice Gas Cellular Automata and Lattice Boltzmann Models* (Springer-Verlag, Berlin, 2000).
[4] S. Succi, *The Lattice Boltzmann Equation for Fluid Dynamics and Beyond* (Clarendon Press, Oxford, 2001).
[5] J. C. Maxwell, Philos. Trans. R. Soc. London **170**, 231 (1879).
[6] M. Smoluchowski, Ann. Phys. Chem. **64**, 101 (1898).
[7] W. G. Vincenti and C. H. Kruger, *Introduction to Physical Gas Dynamics* (John Wiley and Sons, New York, 1965).
[8] G. E. Karniadakis and A. Beskok, *Micro Flows: Fundamentals and Simulation* (Springer-Verlag, New York, 2002).
[9] Y. Sone, *Kinetic Theory and Fluid Dynamics* (Birkhäuser, Boston, 2002).
[10] M. Gad-el-Haq, ASME J. Fluids Eng. **121**, 5 (1999).
[11] J. M. Reese, M. A. Gallis, and D. A. Lockerby, Philos. Trans. R. Soc. London, Ser. A **361**, 2967 (2003).
[12] E. S. Oran, C. K. Oh, and B. Z. Cybyk, Annu. Rev. Fluid Mech. **30**, 403 (1998).
[13] G. Mo and F. Rosenberger, Phys. Rev. A **44**, 4978 (1991).
[14] J. Koplik and J. R. Banavar, Phys. Rev. Lett. **80**, 5125 (1998).
[15] C. Cercignani, *Rarefied Gas Dynamics: From Basic Concepts to Actual Calculations* (Cambridge University Press, Cambridge, England, 2000).
[16] M. Watari and M. Tsutahara, Phys. Rev. E **67**, 036306 (2003).
[17] L. Mieussens, Math. Models Meth. Appl. Sci. **10**, 1121 (2000).
[18] L. Mieussens, J. Comput. Phys. **162**, 429 (2000).
[19] N. Cao, S. Chen, S. Jin, and D. Martinez, Phys. Rev. E **55**, R21 (1997).
[20] R. Mei and W. Shyy, J. Comput. Phys. **143**, 426 (1998).
[21] T. Seta, K. Kono, D. Martinez, and S. Chen, JSME Int. J., Ser. B **43**, 305 (2000).
[22] T. H. Lee and C. L. Lin, J. Comput. Phys. **171**, 336 (2001).
[23] V. Sofonea and R. F. Sekerka, J. Comput. Phys. **184**, 422 (2003).
[24] R. D. Present, *Kinetic Theory of Gases* (McGraw-Hill, Inc., New York, 1958).
[25] V. Sofonea and R. F. Sekerka, Physica A **299**, 494 (2001).
[26] G. R. McNamara, A. L. Garcia, and B. J. Alder, J. Stat. Phys. **81**, 395 (1995).
[27] M. Watari (private communication).
[28] R. Cornubert, D. d'Humières, and D. Levermore, Physica D **47**, 241 (1991).
[29] I. Ginzbourg and P. M. Adler, J. Phys. II **4**, 191 (1994).
[30] A. J. C. Ladd, J. Fluid Mech. **271**, 285 (1994).
[31] E. F. Toro, *Riemann Solvers and Numerical Methods for Fluid Dynamics*, 2nd ed. (Springer-Verlag, Berlin, 1999).
[32] R. J. LeVeque, *Numerical Methods for Conservation Laws* (Birkhäuser Verlag, Basel, 1992).
[33] W. Marques, G. M. Kremer, and F. M. Sharipov, Continuum Mech. Thermodyn. **12**, 379 (2000).
[34] A. Cristea and V. Sofonea, Int. J. Mod. Phys. C **14**, 1251 (2003).
[35] A. Cristea and V. Sofonea, Cent. Eur. J. Phys. **2**, 382 (2004).
[36] V. Sofonea, A. Lamura, G. Gonnella, and A. Cristea, Phys. Rev. E **70**, 046702 (2004).
[37] S. Balay, K. Buschelman, V. Eijkhout, W. Gropp, D. Kaushik, M. Knepley, L. C. McInnes, B. Smith, and H. Zhang, Tech. Rep. ANL-95/11-Revision 2.2.1, Argonne National Laboratory, http://www. mcs. anl. gov/petsc (2004).